Absolute Calibration of Imaging Sensors

DJEDJIGA BELFADEL

Despite the efforts for precise alignment of satellite-based imaging sensors before launch, several factors may cause the values of the calibration parameters to vary between the time of ground calibration and on-orbit operation. This paper considers the problem of satellite-based imaging sensors on-board calibration while estimating the position and velocity of a target of opportunity. The pixel measurements (estimated location of the target's image in the focal-plane array) generated by these sensors are used to estimate the sensors' pointing angle biases, which is a key element of accurate tracking of a target in a space-based system. The target is assumed to be seen by the sensors from a changing direction as a function of the target position, allowing the target in this nonlinear tracking system to be observable. The evaluation of the corresponding Cramér–Rao lower bound on the covariance of the bias estimates and the statistical tests on the results of simulations show that both the target trajectory and the biases are observable and that this method is statistically efficient.

Manuscript received December 28, 2022; revised April 13, 2023; released for publication May 29, 2023.

The author is with the Electrical and Biomedical Engineering, Fairfield University, Fairfield, CT 06824, USA (e-mail: dbelfadel@fairfield.edu).

1557-6418/23/$17.00

I. INTRODUCTION

Image registration is an important research topic in many related areas, such as computer vision, automatic object detection, remote sensing, image processing, robotics, and medical imaging. Multisensor image fusion is the process of combining relevant information from several images into one image. The final output image can provide more information than any of the single images.

In the literature of computer vision, several camera calibration methods exist. These methods are classified based on the calibration object used, such as stereo calibration, plane calibration [13], line calibration [14], and self-calibration [10]. However, it is important to note that constraint conditions become weaker and precision decreases when the dimension is reduced. Thus, if high-precision results are necessary, the latter two methods may not be suitable. Furthermore, the three-dimensional calibration block required for the third method is challenging to make. Therefore, the plane calibration method is a widely used method in computer vision due to its flexibility and simplicity [13].

In order to carry out image fusion, registration error correction is crucial in multisensor systems. This requires estimation of the sensor measurement biases. Measurement bias in target tracking problems can result from a number of different sources. Some primary sources of bias errors include measurement biases due to the deterioration of initial sensor calibration over time, attitude errors caused by biases in the gyros of the inertial measurement units of (airborne or spaceborne) sensors, and timing errors due to the biases in the onboard clock of each sensor platform [9].

For angle-only sensors, imperfect registration leads to line-of-sight (LOS) angle measurement biases in azimuth and elevation. If not corrected, the registration errors can seriously degrade the global surveillance system's performance by increasing tracking errors and even introducing ghost targets. In [7], the effect of sensor and timing bias error on the tracking quality of a space-based infrared (IR) tracking system that utilizes a linearized Kalman filter (LKF) for the highly nonlinear problem of tracking a ballistic missile was presented. This was extended in [8] by proposing a method of using stars observed in the sensor background to reduce the sensor bias error. In [5] simultaneous sensors bias and targets position estimation using fixed passive sensors was proposed. A solution to the related observability issues discussed in [5] was proposed in [6] using space-based sensors. In [4], a simultaneous target state and passive sensor bias estimation were proposed.

In this paper, imaging sensor bias estimation is investigated when only a single target of opportunity is available. The tracking system consists of two or three satellites tracking a ballistic target. The sensors provide synchronized focal-plane (pixel) measurements. The data association is assumed to be correct, and the sensors'

locations are known, and we estimate their orientation biases while simultaneously estimating the state of the target (position and velocity). Our new bias estimation method is validated using a hypothetical scenario created using the System Tool Kit (STK) [1]. Two cases are considered. In the first case, we use three imaging sensors to estimate the state of a ballistic target simultaneously with the biases of the three sensors. In the second case, we estimate the position and velocity of a single target of opportunity simultaneously with the biases of two imaging sensors [3].

First, we discuss the bias estimation for synchronously biased imaging sensors in pixel coordinates. Then we evaluate the corresponding Cramér–Rao lower bound (CRLB) on the covariance of the bias estimates, which is the quantification of the available information on the sensor biases, and show via statistical tests that the estimation is statistically efficient—it meets the CRLB. Section II describes the problem formulation and solution in detail. Section III describes the simulations performed and gives the results. Finally, Section IV gives the conclusions.

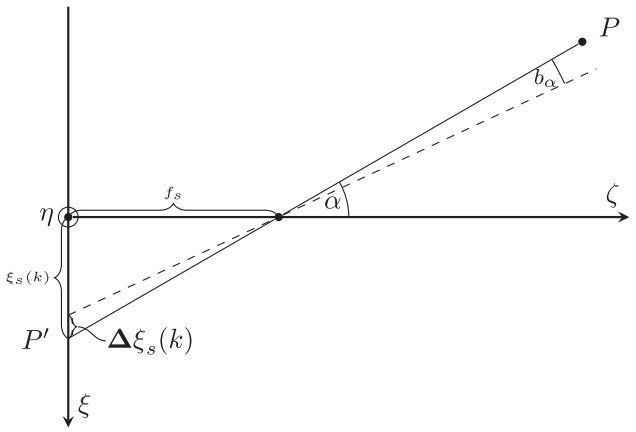

Fig. 1. Sensor coordinates and azimuth pointing bias.

II. PROBLEM FORMULATION

To locate a target in world coordinates and to estimate and correct the biases, one needs to transform the pixels on the image plane to positions in world coordinates and vice versa. Starting with a discussion on the orientation of a spaceborne sensor, this section is devoted to defining the transformations used in the formulation of the new method. The fundamental frame of reference used in this paper is the Earth-centered inertial (ECI) coordinate system. The ECI is defined by the orthogonal set of unit vectors (i_x, i_y, i_z). In a multisensor scenario, sensor platforms will typically have a sensor reference frame associated with them (measurement frame of the sensor) defined by the orthogonal set of unit vectors (i_{xs}, i_{ys}, i_{zs}). The origin of the measurement frame of the sensor is a translation of the ECI origin, and its axes are rotated with respect to the ECI axes. The rotation between these frames can be described by a set of Euler angles. We will refer to these angles $\alpha+\alpha^{\mathrm{n}}$, $\epsilon+\epsilon^{\mathrm{n}}$, $\rho+\rho^{\mathrm{n}}$ of the sensor, as pitch, yaw, and roll, respectively, where α^{n} is the nominal pitch angle, α is the pitch bias, etc. Each angle defines a rotation about a prescribed axis in order to align the sensor frame axes with the ECI axes. The xyz rotation sequence is chosen, which is accomplished by first rotating about the x axis by α^{n}, then rotating about the y axis by ϵ^{n}, and finally rotating about the z axis by ρ^{n}. The rotation sequence can be expressed as

$$
\begin{aligned}
T(\rho^{\mathrm{n}}, \epsilon^{\mathrm{n}}, \alpha^{\mathrm{n}}) &= T_z(\rho^{\mathrm{n}})T_y(\epsilon^{\mathrm{n}})T_x(\alpha^{\mathrm{n}}) \\
&\triangleq \begin{bmatrix} \cos\rho^{\mathrm{n}}\cos\epsilon^{\mathrm{n}} & \cos\rho^{\mathrm{n}}\sin\epsilon^{\mathrm{n}}\sin\alpha^{\mathrm{n}} - \sin\rho^{\mathrm{n}}\cos\alpha^{\mathrm{n}} & \cos\rho^{\mathrm{n}}\sin\epsilon^{\mathrm{n}}\cos\alpha^{\mathrm{n}} + \sin\rho^{\mathrm{n}}\sin\alpha^{\mathrm{n}} \\ \sin\rho^{\mathrm{n}}\cos\epsilon^{\mathrm{n}} & \sin\rho^{\mathrm{n}}\sin\epsilon^{\mathrm{n}}\sin\alpha^{\mathrm{n}} + \cos\rho^{\mathrm{n}}\cos\alpha^{\mathrm{n}} & \sin\rho^{\mathrm{n}}\sin\epsilon^{\mathrm{n}}\cos\alpha^{\mathrm{n}} - \cos\psi_s\sin\alpha^{\mathrm{n}} \\ -\sin\epsilon^{\mathrm{n}} & \cos\epsilon^{\mathrm{n}}\sin\alpha^{\mathrm{n}} & \cos\epsilon^{\mathrm{n}}\cos\alpha^{\mathrm{n}} \end{bmatrix}. \qquad (1)
\end{aligned}
$$

Assume there are N_S synchronized passive sensors with known positions in ECI coordinates, $\mathbf{sp}_s(k) = [e_s(k), n_s(k), u_s(k)]'$, $s = 1, 2, \ldots, N_S$, $k = 0, 1, 2, \ldots, K$, tracking a single target at unknown positions $\mathbf{x}(k) = [x(k), y(k), z(k)]'$, also in ECI coordinates. With the previous convention, the operations needed to transform the position of the target location expressed in ECI coordinates into the sensor s coordinate system (based on its nominal orientation) is

$$
\begin{aligned}
\mathbf{x}_s^{\mathrm{n}}(k) &= T(\omega_s(k))(\mathbf{x}(k) - \mathbf{sp}_s(k)) \\
&\qquad s = 1, 2, \ldots, N_S, \quad k = 0, 1, 2, \ldots, K, \qquad (2)
\end{aligned}
$$

where $\omega_s(k) = [\alpha_s^{\mathrm{n}}(k), \epsilon_s^{\mathrm{n}}(k), \rho_s^{\mathrm{n}}(k)]'$ is the nominal orientation of sensor s, $T(\omega_s(k))$ is the appropriate rotation matrix, and the translation $(\mathbf{x}(k) - \mathbf{sp}_s(k))$ is the difference between the vector position of the target and the vector position of the sensor s, both expressed in ECI coordinates. The superscript "n" in (2) indicates that the rotation matrix is based on the nominal sensor orientation.

A. Measurement Model

In the process of optical imaging, a simplified model of image formation is shown in Fig. 1. In this so-called pinhole camera model, the lens is a single point. A given scene is mapped onto the image plane by projection through the optical center of the imaging lens. We shall define the sensor coordinate system as having the horizontal and vertical axes of the image plane labeled ξ

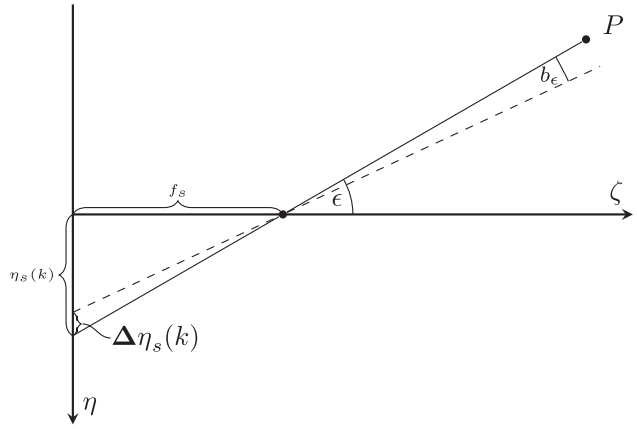

Fig. 2. Sensor coordinates and elevation pointing bias.

and η, respectively, and the "optical axis", labeled ζ (as shown in Figs. 1 and 2). Assume that the origin of the sensor coordinate system is the lens center, and f_s is the focal length of the optical sensor, the distance from the lens focal point to the image plane. The three-dimensional coordinates $(x_s(k), y_s(k), z_s(k))$ of a point target are transformed to the image coordinates $(\xi_s(k), \eta_s(k))$ under perspective projection. Then using the two similar triangles, we can write the $\xi_s(k)$ image coordinate in the focal plane as

$$\xi_s(k) = -f_s \frac{x_s(k)}{z_s(k)}, \tag{3}$$

where f_s is the focal length of sensor s and the negative sign is due to the reversing of the image. Similarly, as shown in Fig. 2, the $\eta_s(k)$ coordinate of the image is given by

$$\eta_s(k) = -f_s \frac{y_s(k)}{z_s(k)}. \tag{4}$$

For our bias estimation algorithm, the target measurements will be generated in pixels $\xi_s(k)$ and $\eta_s(k)$. For convenience, the xzy coordinate system is used, the azimuth angle $\beta_s(k)$ is taken in the sensor xz plane between the sensor z axis and the line of sight to the target, while the elevation angle $\gamma_s(k)$ is the angle taken in the Cartesian plane yz between the z axis and the line of sight to the target, that is,

$$\begin{bmatrix} \beta_s(k) \\ \gamma_s(k) \end{bmatrix} = \begin{bmatrix} \tan^{-1}\left(\frac{x_s(k)}{z_s(k)}\right) \\ \tan^{-1}\left(-\frac{y_s(k)}{\sqrt{x_s^2(k)+z_s^2(k)}}\right) \end{bmatrix}. \tag{5}$$

Assuming a small clockwise roll of b_ρ about the ζ axis, the resulting tilted (rotated) image has the focal plane coordinates

$$\xi_s'(k) = \xi_s(k)\cos b_{\rho_s} + \eta_s(k)\sin b_{\rho_s}, \tag{6}$$

$$\eta_s'(k) = -\xi_s(k)\sin b_{\rho_s} + \eta_s(k)\cos b_{\rho_s}, \tag{7}$$

where $\xi_s'(k)$ and $\eta_s'(k)$ are the resulting pixel positions after the rolling, and $\xi_s(k)$ and $\eta_s(k)$ are the ideal image positions. As shown in Fig. 1, the azimuth bias b_{α_s} of sensor s results in a horizontal bias in pixels of

$$\begin{aligned} \Delta\xi_s(k) &= \frac{f_s \sin b_{\alpha_s}}{\cos\alpha_s(k)\cos(\alpha_s(k) - b_{\alpha_s})} \\ &= \frac{f_s \sin b_{\alpha_s}}{\cos\alpha_s(k)(\cos\alpha_s(k)\cos b_{\alpha_s} + \sin\alpha_s(k)\sin b_{\alpha_s})} \\ &= \frac{f_s \sin b_{\alpha_s}}{\cos^2\alpha_s(k)\cos b_{\alpha_s} + \cos\alpha_s(k)\sin\alpha_s(k)\sin b_{\alpha_s}} \\ &= \frac{f_s}{\cos^2\alpha_s(k)\frac{\cos b_{\alpha_s}}{\sin b_{\alpha_s}} + \cos\alpha_s(k)\sin\alpha_s(k)} \\ &= \frac{f_s}{\cos^2\alpha_s(k)\cot b_{\alpha_s} + \cos\alpha_s(k)\sin\alpha_s(k)} \\ &\qquad s = 1, 2, \ldots, N_s. \end{aligned} \tag{8}$$

Similarly, as shown in Fig. 2, the elevation bias b_{ϵ_s} results in a vertical bias in pixels of

$$\begin{aligned} \Delta\eta_s(k) &= \frac{f_s \sin b_{\epsilon_s}}{\cos\epsilon_s(k)\cos(\epsilon_s(k) - b_{\epsilon_s})} \\ &= \frac{f_s}{\cos^2\epsilon_s(k)\cot b_{\epsilon_s} + \cos\epsilon_s(k)\sin\epsilon_s(k)}. \end{aligned} \tag{9}$$

The focal length is related to the horizontal field of view $2\alpha_{\max}$ and N_ξ, the number of pixels along the horizontal ξ axis.

$$f_s = \frac{1}{2} N_\xi \frac{1}{\tan\alpha_{\max}}. \tag{10}$$

Combining (7)–(10), the noiseless biased measurements of the target from sensor s in pixels are

$$\begin{aligned} \xi_s^b(k) = {} & \xi_s(k)\cos b_{\rho_s} \\ & - \frac{f_s}{\cos^2\alpha_s(k)\cot b_{\alpha_s} + \cos\alpha_s(k)\sin\alpha_s(k)} \\ & + \eta_s(k)\sin b_{\rho_s}, \end{aligned} \tag{11}$$

$$\begin{aligned} \eta_s^b(k) = {} & \eta_s(k)\cos b_{\rho_s} \\ & - \frac{f_s}{\cos^2\epsilon_s(k)\cot b_{\epsilon_s} + \cos\epsilon_s(k)\sin\epsilon_s(k)} \\ & - \xi_s(k)\sin b_{\rho_s}, \end{aligned} \tag{12}$$

where $\xi_s(k)$ and $\eta_s(k)$ are the ideal image pixel positions. b_{α_s}, b_{ϵ_s}, and b_{ρ_s} are the azimuth, elevation, and roll biases, respectively. The model for the biased noise free focal-plane measurements expressed in pixels is

then

$$\mathbf{h}\left(\mathbf{x}_s(k), \mathbf{b}_s\right) = \begin{bmatrix} \boldsymbol{\xi}_s^b(k) \\ \eta_s^b(k) \end{bmatrix} = \begin{bmatrix} \xi_s(k)\cos b_{\rho_s} - \frac{f_s}{\cos^2\alpha_s(k)\cot b_{\alpha s}+\cos\alpha_s(k)\sin\alpha_s(k)} + \eta_s(k)\sin b_{\rho_s} \\ \eta_s(k)\cos b_{\rho_s} - \frac{f_s}{\cos^2\epsilon_s(k)\cot b_{\epsilon_s}+\cos\epsilon_s(k)\sin\epsilon_s(k)} - \xi_s(k)\sin b_{\rho_s} \end{bmatrix}$$

$$= \begin{bmatrix} -\frac{f_s x_s(k)}{z_s(k)}\cos b_{\rho_s} - \frac{f_s}{\frac{z_s^2(k)}{x_s^2(k)+z_s^2(k)}\cot b_{\alpha_s}+\frac{x_s(k)z_s(k)}{x_s^2(k)+z_s^2(k)}} - \frac{f_s y_s(k)}{z_s(k)}\sin b_{\rho_s} \\ -\frac{f_s y_s(k)}{z_s(k)}\cos b_{\rho_s} - \frac{f_s}{\frac{x_s^2(k)+z_s^2(k)}{x_s^2(k)+y_s^2(k)+z_s(k)}\cot b_{\epsilon_s}+\frac{z_s(k)\sqrt{x_s^2(k)+z_s^2(k)}}{x_s^2(k)+y_s^2(k)+z_s^2(k)}} + \frac{f_s x_s(k)}{z_s(k)}\sin b_{\rho_s} \end{bmatrix}$$

$$= f_s \begin{bmatrix} -\frac{x_s(k)}{z_s(k)}\cos b_{\rho_s} - \frac{y_s(k)}{z_s(k)}\sin b_{\rho_s} - \frac{x_s^2(k)+z_s^2(k)}{z_s^2(k)\cot b_{\alpha_s}+x_s(k)z_s(k)} \\ -\frac{y_s(k)}{z_s(k)}\cos b_{\rho_s} + \frac{x_s(k)}{z_s(k)}\sin b_{\rho_s} - \frac{x_s^2(k)+y_s^2(k)+z_s^2(k)}{(x_s^2(k)+z_s^2(k))\cot b_{\epsilon_s}+z_s(k)\sqrt{x_s^2(k)+z_s^2(k)}} \end{bmatrix}, \tag{13}$$

where $[\xi_s(k)\ \ \eta_s(k)]'$ is the focal-plane position of the image of the target seen by sensor s, $\mathbf{x}_s(k) = [x_s(k), y_s(k), z_s(k)]$ is the target position, and $\mathbf{b}_s = [b_{\alpha_s}\ b_{\epsilon_s}\ b_{\rho_s}]'$ is the bias vector of sensor s.

At time k, each sensor provides the noisy measurements

$$\mathbf{z}_s(k) = \mathbf{h}_s\left(\mathbf{x}_s(k), \mathbf{b}_s\right) + \mathbf{w}_s(k), \tag{14}$$

Let $\mathbf{z}$ be an augmented vector consisting of the batch-stacked measurements from all the sensors up to time K

$$\mathbf{z} = [z_1(1), z_2(1), \ldots, z_{N_S}(1), \ldots, z_1(K), z_2(K), \ldots, z_{N_S}(K)], \tag{15}$$

and

$$\mathbf{w}_s(k) = \left[w_s^{\xi}(k), w_s^{\eta}(k)\right]'. \tag{16}$$

The measurement noises $\mathbf{w}_s(k)$ are zero-mean, white Gaussian with

$$R_s = \begin{bmatrix} (\sigma_s^{\xi})^2 & 0 \\ 0 & (\sigma_s^{\eta})^2 \end{bmatrix} \quad s = 1, 2, \ldots, N_S \tag{17}$$

and are assumed mutually independent.

The problem is to estimate the bias vectors for all sensors and the state vector (position and velocity) of the target of opportunity, i.e.,

$$\theta = [x(K), y(K), z(K), \dot{x}(K), \dot{y}(K), \dot{z}(K), \mathbf{b}_1', \ldots, \mathbf{b}_{N_S}']' \tag{18}$$

from

$$\mathbf{z} = \mathbf{h}(\theta) + \mathbf{w}, \tag{19}$$

where

$$\mathbf{h}(\theta) = [h_{11}(\theta)', h_{21}(\theta)', \ldots, h_{N_S 1}(\theta)', \ldots, h_{1K}(\theta)', h_{2K}(\theta)', \ldots, h_{N_S K}(\theta)']', \tag{20}$$

$$\mathbf{w} = [\mathbf{w}_1(1)', \mathbf{w}_2(1)', \ldots, \mathbf{w}_{N_S}(1)', \ldots, \mathbf{w}_1(K)', \mathbf{w}_2(K)', \ldots, \mathbf{w}_{N_S}(K)']', \tag{21}$$

and the covariance of the stacked process noise (21) is the $(N_S K \times N_S K)$ block-diagonal matrix

$$R = \begin{bmatrix} R_1 & 0 & \cdots & 0 \\ 0 & R_2 & \cdots & 0 \\ \vdots & \vdots & \ddots & \vdots \\ 0 & \cdots & 0 & R_{N_S} \end{bmatrix}. \tag{22}$$

We shall obtain the maximum likelihood (ML) estimate of the augmented parameter vector (18), consisting of the (unknown) target position, velocity, and sensor biases, by maximizing the likelihood function (LF) of θ based on $\mathbf{z}$

$$\Lambda(\theta; \mathbf{z}) = p\left(\mathbf{z}|\theta\right), \tag{23}$$

where

$$p\left(\mathbf{z}|\theta\right) = |2\pi R|^{-1/2} \exp\left(-\frac{1}{2}\left[\mathbf{z} - \mathbf{h}\left(\theta\right)\right]' R^{-1}\left[\mathbf{z} - \mathbf{h}\left(\theta\right)\right]\right), \tag{24}$$

and $\mathbf{h}$ is defined in (20)

The ML estimate (MLE) is then

$$\hat{\theta}(\mathbf{z})^{\mathrm{ML}} = \arg\max_{\theta} \Lambda(\theta; \mathbf{z}). \tag{25}$$

In order to find the MLE, one has to solve a nonlinear least squares problem. This will be done using a numerical search via the batch iterated least squares (ILS) technique.

B. Space Target Dynamics

The state-space model for a noiseless discrete-time system[1] is of the general form

$$\mathbf{x}(k+1) = f[\mathbf{x}(k), \mathbf{u}(k)] \quad k = 0, 1, 2, \ldots, K-1. \tag{26}$$

With small time steps ($\leq$10 s), we can approximate the motion model with the discrete-time dynamic equation

$$\mathbf{x}(k+1) = F\mathbf{x}(k) + G\mathbf{u}(k), \tag{27}$$

[1]Since we are dealing with exoatmospheric motion, it is reasonable to assume that it is noiseless.

where

$$\mathbf{x}(k) = [x(k), y(k), z(k), \dot{x}(k), \dot{y}(k), \dot{z}(k)]', \quad k = 0, 1, 2, \ldots, K \tag{28}$$

is the six-dimensional state vector at time k, F is the state-transition matrix, and $\mathbf{u}$ is a known input representing the gravitational effects acting on the target [given in (31)]. The state-transition matrix for a target with acceleration due to gravity is

$$F = \begin{bmatrix} 1 & 0 & 0 & \Delta t & 0 & 0 \\ 0 & 1 & 0 & 0 & \Delta t & 0 \\ 0 & 0 & 1 & 0 & 0 & \Delta t \\ 0 & 0 & 0 & 1 & 0 & 0 \\ 0 & 0 & 0 & 0 & 1 & 0 \\ 0 & 0 & 0 & 0 & 0 & 1 \end{bmatrix}, \tag{29}$$

and the known input gain matrix (multiplying the appropriate components of the gravity vector) is

$$G = \begin{bmatrix} \Delta t^2/2 & 0 & 0 \\ 0 & \Delta t^2/2 & 0 \\ 0 & 0 & \Delta t^2/2 \\ \Delta t & 0 & 0 \\ 0 & \Delta t & 0 \\ 0 & 0 & \Delta t \end{bmatrix}, \tag{30}$$

where Δt is the sampling interval. The gravity term is given by

$$\mathbf{u}(k) = g\frac{\mathbf{x}_{\mathrm{p}}(k)}{a(\mathbf{x}_{\mathrm{p}}(k))}, \tag{31}$$

where $\mathbf{x}_{\mathrm{p}}$ is the position part of the state $\mathbf{x}$ in (28), $g = 9.8\ \mathrm{m/s^2}$, and

$$a = \sqrt{x(k)^2 + y(k)^2 + z(k)^2} \tag{32}$$

is the distance from the target to the origin of the coordinates system. For simplicity, we assume g to be constant. The ratio $\mathbf{x}_{\mathrm{p}}/a$ yields the time-varying components of the gravity acting on the target and provides the scaling factor for the gravity term. Note that in view of (31), the state model (27) is not linear.

C. Bias Estimability

Intuitively, the observability of a system guarantees that the sensor measurements provide sufficient information for estimating the unknown parameters. As discussed in [4], the two requirement for bias estimability are:

First Requirement for Bias Estimability: Each sensor provides a two-dimensional measurement (the two pixel positions of the target in the sensor image) at time K. We assume that each sensor sees the target at all the times $0, 1, 2, \ldots, K$. Stacking together all the measurements results in an overall measurement vector of dimension $2KN_S$. Given that the position, velocity of the target, and bias vectors of each sensor are three-dimensional, and knowing that the number of equations (size of the stacked measurement vector) has to be at least equal to the number of parameters to be estimated (target state and biases), we must have

$$2KN_S \geq 3N_S + 6. \tag{33}$$

This is a necessary condition but not sufficient because (25) has to have a unique solution, i.e., the parameter vector has to be estimable. This is guaranteed by the second requirement.

Second Requirement of Bias Estimability: This is the invertibility of the Fisher information matrix (FIM). In order to have parameter observability, the FIM must be invertible. If the FIM is not invertible (i.e., it is singular), then the CRLB (the inverse of the FIM) will not exist—the FIM will have one or more infinite eigenvalues, which means total uncertainty in a subspace of the parameter space, i.e., ambiguity [2].

For the example of bias estimability discussed in the sequel, estimate the biases of 2 sensors (6 bias components) and 6 target components (3 position and 3 velocity components), i.e., the search is in a 12-dimensional space in order to meet the necessary requirement (33). As stated previously, the FIM must be invertible, so the rank of the FIM has to be equal to the number of parameters to be estimated ($6 + 6 = 12$ in the previous example). The full rank of the FIM is a necessary and sufficient condition for estimability. There exists, however, a subtle unobservability for this example that will necessitate the use of more measurements than the strict minimum number of measurements given by (33).

D. Iterated Least Squares for Maximization of the LF of θ

Given the estimate $\hat{\theta}^j$ after j iterations, the batch ILS estimate after the $(j+1)$th iteration will be

$$\hat{\theta}^{j+1} = \hat{\theta}^j + [(H^j)'R^{-1}H^j]^{-1}(H^j)'R^{-1}[\mathbf{z} - \mathbf{h}(\hat{\theta}^j)], \tag{34}$$

where

$$\mathbf{h}(\hat{\theta}^j) = [h_{11}(\hat{\theta}^j)', h_{21}(\hat{\theta}^j)', \ldots, h_{N_s1}(\hat{\theta}^j)', \ldots, h_{1K}(\hat{\theta}^j)', h_{2K}(\hat{\theta}^j)', \ldots, h_{N_sK}(\hat{\theta}^j)'], \tag{35}$$

where

$$H^j = \left.\frac{\partial \mathbf{h}\left(\theta^j\right)}{\partial \theta}\right|_{\theta=\hat{\theta}^j} \tag{36}$$

is the Jacobian matrix of the vector consisting of the stacked measurement functions (35) w.r.t. (18) evaluated at the ILS estimate from the previous iteration j. In this case, the Jacobian matrix is, with the iteration index omitted for conciseness,

$$H = \left[\, H_{11}\ H_{21}\ H_{N_s1} \cdots H_{1K}\ H_{2K}\ H_{N_sK} \,\right]', \tag{37}$$

where

$$H_s(k) = \begin{bmatrix} \frac{\partial \xi_s(k)}{\partial x(k)} & \frac{\partial \xi_s(k)}{\partial y(k)} & \frac{\partial \xi_s(k)}{\partial z(k)} & \frac{\partial \xi_s(k)}{\partial \dot{x}(k)} & \frac{\partial \xi_s(k)}{\partial \dot{y}(k)} & \frac{\partial \xi_s(k)}{\partial \dot{z}(k)} & \frac{\partial \xi_s(k)}{\partial b_{\alpha_1}} & \frac{\partial \xi_s(k)}{\partial b_{\epsilon_1}} & \frac{\partial \xi_s(k)}{\partial b_{\rho_1}} & \cdots & \frac{\partial \xi_s(k)}{\partial b_{\alpha_{N_S}}} & \frac{\partial \xi_s(k)}{\partial b_{\epsilon_{N_S}}} & \frac{\partial \xi_s(k)}{\partial b_{\rho_{N_S}}} \\ \frac{\partial \eta_s(k)}{\partial x(k)} & \frac{\partial \eta_s(k)}{\partial y(k)} & \frac{\partial \eta_s(k)}{\partial z(k)} & \frac{\partial \eta_s(k)}{\partial \dot{x}(k)} & \frac{\partial \eta_s(k)}{\partial \dot{y}(k)} & \frac{\partial \eta_s(k)}{\partial \dot{z}(k)} & \frac{\partial \eta_s(k)}{\partial b_{\epsilon_1}} & \frac{\partial \eta_s(k)}{\partial b_{\epsilon_1}} & \frac{\partial \eta_s(k)}{\partial b_{\rho_1}} & \cdots & \frac{\partial \eta_s(k)}{\partial b_{\epsilon_{N_S}}} & \frac{\partial \eta_s(k)}{\partial b_{\epsilon_{N_S}}} & \frac{\partial \eta_s(k)}{\partial b_{\rho_{N_S}}} \end{bmatrix}, \quad (38)$$

The appropriate partial derivatives, in pixel measurements, with respect to the target position and velocity components are given in the appendix.

E. Initial Solution

Assuming that the biases are null, the LOS measurements from the first and second sensors $\alpha_1(k), \alpha_2(k)$, and $\epsilon_1(k)$ can be used to solve for each initial Cartesian target position in ECI coordinates using (39)–(41). The two Cartesian positions formed from (39) to (41) can then be differenced to provide an approximate velocity. This procedure is analogous to two-point differencing [2] and will provide a full six-dimensional state to initialize the ILS algorithm.

$$x(k)^0 = \frac{y_2(k) - y_1(k) + x_1(k)\tan\alpha_1(k) - x_2(k)\tan\alpha_2(k)}{\tan\alpha_1(k) - \tan\alpha_2(k)}, \quad (39)$$

$$y(k)^0 = \frac{\tan\alpha_1(k)\,(y_2(k) + \tan\alpha_2(k)\,(x_1(k) - x_2(k))) - y_1(k)\tan\alpha_2(k)}{\tan\alpha_1(k) - \tan\alpha_2(k)}, \quad (40)$$

$$z(k)^0 = z_1(k) + \tan\epsilon_1(k) \times \left| \frac{(y_1(k) - y_2(k))\cos\alpha_2(k) + (x_2(k) - x_1(k))\sin\alpha_2(k)}{\sin(\alpha_1(k) - \alpha_2(k))} \right| \quad k = 1, 2, \ldots, K. \quad (41)$$

The CRLB provides a lower bound on the covariance matrix of an unbiased estimator [2] as

$$E\{(\boldsymbol{\Theta} - \hat{\boldsymbol{\Theta}})(\boldsymbol{\Theta} - \hat{\boldsymbol{\Theta}})'\} \geq J(\boldsymbol{\Theta})^{-1}, \quad (42)$$

where $\boldsymbol{\Theta}$ is the true parameter vector to be estimated, $\hat{\boldsymbol{\Theta}}$ is the estimate, and J is the FIM given as

$$J(\boldsymbol{\Theta}) = E\left\{[\nabla_{\boldsymbol{\Theta}} \ln \Lambda(\boldsymbol{\Theta})]\,[\nabla_{\boldsymbol{\Theta}} \ln \Lambda(\boldsymbol{\Theta})]'\right\}\Big|_{\boldsymbol{\Theta}=\boldsymbol{\Theta}_{\text{true}}} = \Delta'\left(R^{-1}\right)\Delta\Big|_{\boldsymbol{\Theta}=\boldsymbol{\Theta}_{\text{true}}}, \quad (43)$$

where Δ is given by (37) and R given by (22).

F. Statistical Test for Efficiency With Monte Carlo Runs

As discussed in [2], the normalized estimation error squared (NEES) for the parameter $\boldsymbol{\Theta}$ (under the hypothesis of efficiency), defined as

$$\gamma_{\boldsymbol{\Theta}} = (\boldsymbol{\Theta} - \hat{\boldsymbol{\Theta}})' P^{-1} (\boldsymbol{\Theta} - \hat{\boldsymbol{\Theta}}) = (\boldsymbol{\Theta} - \hat{\boldsymbol{\Theta}})' J(\boldsymbol{\Theta})(\boldsymbol{\Theta} - \hat{\boldsymbol{\Theta}}) \quad (44)$$

is Chi-square distributed with $n_{\boldsymbol{\Theta}}$ (the dimension of $\boldsymbol{\Theta}$) degrees of freedom, assuming that estimation errors are Gaussian, that is,

$$\gamma_{\boldsymbol{\Theta}} \sim \chi^2_{n_{\boldsymbol{\Theta}}}. \quad (45)$$

The hypothesis test whether efficiency can be accepted, i.e., that $P = J^{-1}$, is discussed in [2] and outlined next. The NEES is used in simulations to check whether the estimator is efficient. In practice, to check the estimator efficiency, we use the sample average NEES from N independent Monte Carlo runs, defined as

$$\bar{\gamma}_{\boldsymbol{\Theta}} = \frac{1}{N}\sum_{i=1}^{N} \gamma^i_{\boldsymbol{\Theta}}. \quad (46)$$

The quantity $N\bar{\gamma}_{\boldsymbol{\Theta}}$ is Chi-square distributed with $Nn_{\boldsymbol{\Theta}}$ degrees of freedom.

III. SIMULATIONS

We simulate a space-based tracking system tracking a ballistic missile. The missile and satellite trajectories are generated using STK.[2] The target modeled represents a ballistic missile with a flight time of about 20 min. STK provides the target and sensor positions in three-dimensional Cartesian coordinates at 1 s intervals. The target launch time is chosen so that the satellite sensors are able to follow the missile's trajectory throughout its flight path. The missile and satellite trajectories represent 5 min of flight time (exoatmospheric).

A. Three-Sensor Case

We simulated three space-based imaging sensors at various known orbits, observing a target of opportunity at unknown locations. In this case, a 15-dimensional parameter vector is to be estimated. The horizontal and vertical fields of view of each sensor are assumed to be 60°. The measurement noise standard deviation σ_s (identical across sensors for both horizontal and vertical axes of the image plane ξ and η measurements, $\sigma_s^{\xi} = \sigma_s^{\eta} = \sigma_s$) was assumed to be 0.3 pixel. As shown in Fig. 3, these satellite orbits enabled maximum visibility of the missile trajectory from multiple angles. As discussed in the previous section, the three sensor biases are roll, pitch, and yaw angle offsets. Table I summarizes the bias values (in mrad).

[2]STK is registered trademark of Analytical Graphics, Inc.

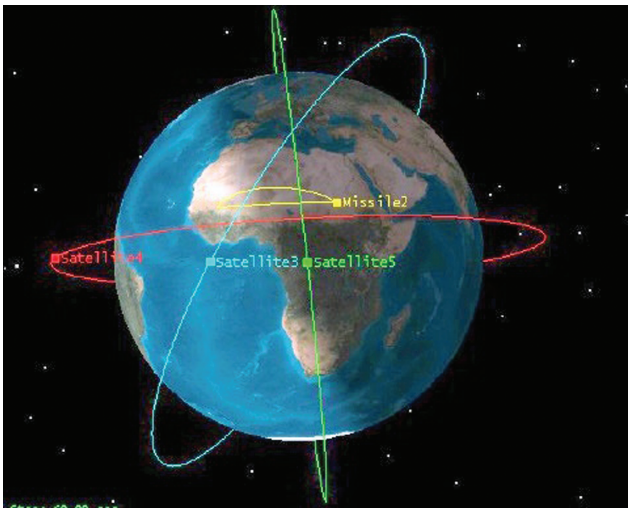

Fig. 3. Target and satellite trajectories for the three-sensor case.

B. Statistical Efficiency of the Estimates for the Three-Sensor Case

In order to test for the statistical efficiency of the estimate [of the 15-dimensional vector (18)], the NEES [2] is used, with the CRLB as the covariance matrix. The sample average NEES over 100 Monte Carlo runs calculated using the FIM evaluated at the true bias values and target locations is approximately 14.3, and the sample average NEES calculated using the FIM evaluated at the estimated biases and target locations is approximately 14.6, and both fall in the interval given below. According to the CRLB, the FIM has to be evaluated at the true parameter. Since this is not available in practice, however, it is useful to evaluate the FIM also at the estimated parameter, the only one available in real-world implementations [11], [12]. The 95% probability region for the 100-sample average NEES of the 15-dimensional parameter vector is [13.95, 16.09]. This NEES is found to be within this interval, and the MLE is therefore statistically efficient. Fig. 4 shows the individual bias component NEES. The 95% probability region for the 100-sample average single component NEES is [0.74, 1.29]. The NEES values are found to be within this interval.

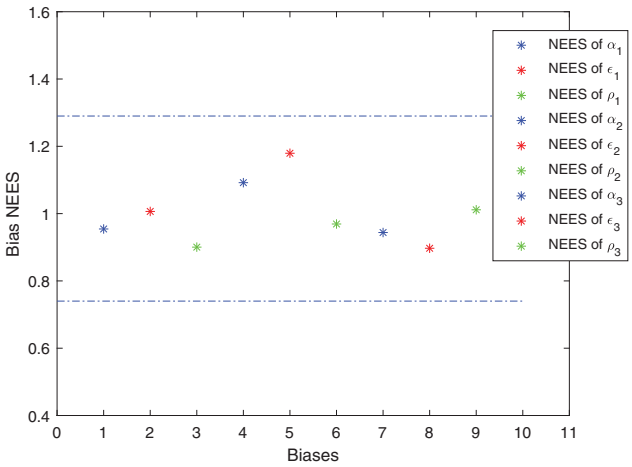

Fig. 4. Sample average bias NEES (CRLB evaluated at the estimate), for each of the nine biases, over 100 Monte Carlo runs (three-sensor case).

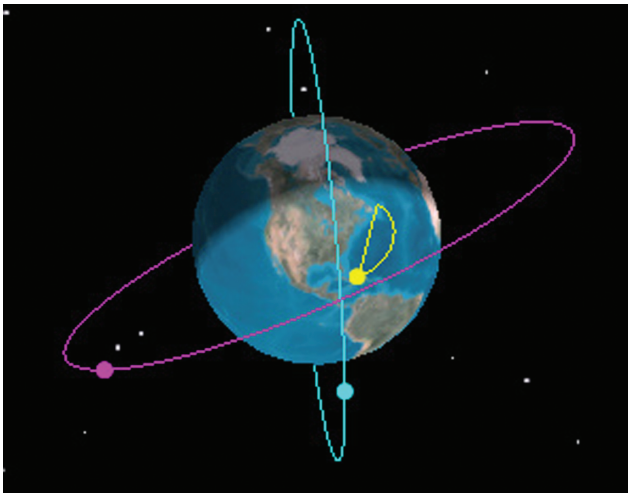

Fig. 5. Target and satellite trajectories for the two-sensor case.

Table I
Sensor Biases (mrad) for the Three-Sensor Case

	α	ϵ	ρ
Sensor 1	2.90	2.80	3.40
Sensor 2	3.33	2.90	3.00
Sensor 3	3.03	3.00	2.90

C. Two-Sensor Case

We simulated two satellite-based imaging sensors at various locations, observing a single target of opportunity. The sensor satellites are in circular orbits of 550 km and 675 km altitude with 0° and 45° inclination, respectively. The horizontal and vertical fields of view of each sensor are assumed to be 60°. The measurement noise standard deviation σ_s (identical across sensors for both horizontal and vertical axes of the image plane ξ and η measurements, $\sigma_s^{\xi} = \sigma_s^{\eta} = \sigma_s$) was assumed to be 0.3 pixel. As shown in Fig. 5, these satellite orbits enabled maximum visibility of the missile trajectory from multiple angles. As discussed in the previous section, the three sensor biases were pitch, yaw, and roll angle offsets. Table II summarizes the bias values (in mrad).

Table II
Sensor Biases (mrad) for the Two-Sensor Case

	α	ϵ	ρ
Sensor 1	2.90	2.80	3.40
Sensor 2	3.33	2.90	3.00

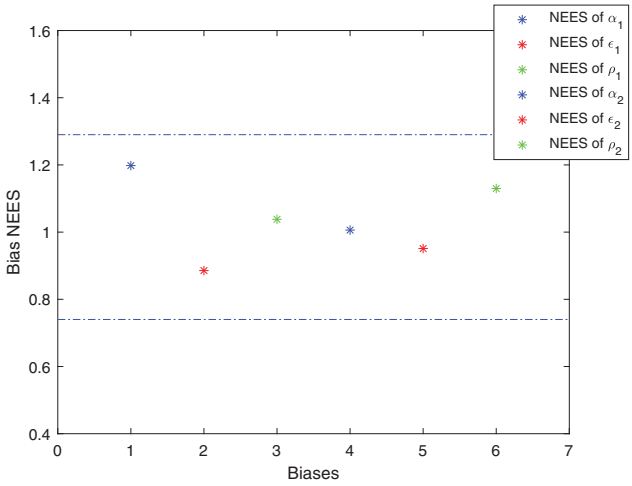

Fig. 6. Sample average bias NEES for each of the six biases.

D. Statistical Efficiency of the Estimate for the Two-Sensor Case

In order to test for the statistical efficiency of the estimate [of the 12-dimensional vector (18)], the NEES is used, with the CRLB as the covariance matrix. The sample average NEES over 100 Monte Carlo runs calculated using the FIM evaluated at the true bias values, target position, and velocity is approximately 11.24, and the sample average NEES calculated using the FIM evaluated at the estimated biases, target position, and velocity is approximately 11.45, both fall in the interval given below. According to the CRLB, the FIM has to be evaluated at the true parameter. Since this is not available in practice, however, it is useful to evaluate the FIM also at the estimated parameter, the only one available in real world implementations [12]. The results are practically identical regardless of which values are chosen for the evaluation of the FIM. The 95% probability region for the 100-sample average NEES of the 12-dimensional parameter vector is [11.20, 12.81]. This NEES is found to be within this interval, and the MLE is therefore statistically efficient. Fig. 6 and Table III show the individual bias component, NEES. The 95% probability region for the 100-sample average single component NEES is [0.74, 1.29]. These NEES are found to be within this interval.

IV. CONCLUSIONS

In this paper, we presented an algorithm that uses a single target of opportunity for the estimation of measurement biases. The first step was deriving a general bias model for synchronized imaging sensors. Based on this derivation, we formulated a nonlinear least-squares estimation scheme for concurrent estimation of the Cartesian position and the velocity in three-dimensional of the target and the angle biases of the sensors. The ILS estimate was shown to be a statistically efficient estimate, and the residual biases are negligible in view of the measurement noise. As such, the covariance matrix from the CRLB can be used as the measurement noise covariance matrix for the resulting composite measurement in a tracking filter. This composite measurement can then be used (with a linear measurement equation) for dynamic state estimation, where position measurements in Cartesian space are preferable to pixel measurements.

Table III
Sample Average Bias NEES (CRLB Evaluated at the Estimate), for Each of the Six Biases, Over 100 Monte Carlo Runs

Biases	α_1	ϵ_1	ρ_1	α_2	ϵ_2	ρ_2
NEES	1.2461	0.9891	1.2043	1.0711	1.0430	0.9734

APPENDIX

The partial derivatives of (38), in pixel measurements, with respect to the target position and velocity components are

$$\frac{\partial \xi_s(k)}{\partial x_s(k)} = -\frac{\cos b_{\rho_s}}{z_s(k)} - \frac{2x_s(k)}{q_1} + \frac{z_s(k)(x_s^2(k)+z_s^2(k))}{{q_1}^2}$$

$$\frac{\partial \xi_s(k)}{\partial y_s(k)} = -\frac{\sin b_{\rho_s}}{z_s(k)}$$

$$\frac{\partial \xi_s(k)}{\partial z_s(k)} = \frac{x_s(k)\cos b_{\rho_s} + y_s(k)\sin b_{\rho_s}}{z_s^2(k)} - \frac{2z_s(k)}{q_1} + \frac{(x_s^2(k)+z_s^2(k))(x_s(k)+2z_s(k)\cot b_{\alpha_s})}{q_1^2}$$

$$\frac{\partial \xi_s(k)}{\partial \dot{x}_s(k)} = \Delta t \frac{\partial \xi_s(k)}{\partial x_s(k)}$$

$$\frac{\partial \xi_s(k)}{\partial \dot{y}_s(k)} = 0$$

$$\frac{\partial \xi_s(k)}{\partial \dot{z}_s(k)} = \Delta t \frac{\partial \xi_s(k)}{\partial z_s(k)}$$

$$\frac{\partial \xi_s(k)}{\partial b_{\alpha_s}} = -\frac{z_s^2(k)(x_s^2(k)+z_s^2(k))}{q_1^2}$$

$$\frac{\partial \xi_s(k)}{\partial b_{\rho_s}} = \frac{x_s(k)\sin b_{\rho_s} + y_s(k)\cos b_{\rho_s}}{z_s(k)}$$

$$\frac{\partial \eta_s(k)}{\partial x_s(k)} = \frac{\sin b_{\rho_s}}{z_s(k)} - \frac{x_s(k)}{r^2 q_2} + \frac{r^2\left(2x_s(k)\cot b_{\epsilon_s} + \frac{x_s(k)z_s(k)}{\sqrt{x_s^2(k)+z_s^2(k)}}\right)}{{q_2}^2}$$

$$\frac{\partial \eta_s(k)}{\partial y_s(k)} = -\frac{\cos b_{\rho_s}}{z_s(k)} - \frac{y_s}{r^2 q_2}$$

$$\frac{\partial \eta_s(k)}{\partial z_s(k)} = \frac{y_s(k)\cos b_{\rho_s} - x_s(k)\sin b_{\rho_s}}{z_s^2(k)}$$

$$+\frac{r^2\left(2z_s(k)\cot b_{\epsilon_s}+\sqrt{x_s^2(k)+z_s^2(k)}+\frac{zs^2}{\sqrt{x_s^2(k)+z_s^2(k)}}\right)}{{q_2}^2}$$

$$-\frac{z_s(k)}{r^2 q_2}$$

$$\frac{\partial \eta_s(k)}{\partial b_{\epsilon_s}}=-\frac{r^2(x_s^2(k)+z_s^2(k))(\cot b_{\epsilon_s}^2+1)}{{q_2}^2}$$

$$\frac{\partial \eta_s(k)}{\partial b_{\rho_s}}=\frac{x_s(k)\cos b_{\rho_s}+y_s(k)\sin b_{\rho_s}}{z_s^2(k)}$$

$$\frac{\partial \eta_s(k)}{\partial \dot{x}_s(k)}=\Delta t\frac{\partial \eta_s(k)}{\partial x_s(k)}$$

$$\frac{\partial \eta_s(k)}{\partial \dot{y}_s(k)}=\Delta t\frac{\partial \eta_s(k)}{\partial y_s(k)}$$

$$\frac{\partial \eta_s(k)}{\partial \dot{z}_s(k)}=\Delta t\frac{\partial \eta_s(k)}{\partial z_s(k)},$$

where

$$q_1=\cot b_{\alpha_s}z_s^2(k)+x_s(k)z_s(k),$$

and

$$q_2=\cot b_{\epsilon_s}(x_s^2(k)+z_s^2(k))+z_s(k)\sqrt{x_s^2(k)+z_s^2(k)}$$

REFERENCES

[1] System Tool Kit, registered trademark of Analytical Graphics Inc., Dec. 2022. [Online]. Available: https://www.agi.com

[2] Y. Bar-Shalom, X.-R. Li, and T. Kirubarajan
Estimation with Applications to Tracking and Navigation: Theory, Algorithms and Software. Hoboken, NJ, USA: Wiley, 2001.

[3] D. Belfadel and Y. Bar-Shalom
"On-orbit calibration of satellite based imaging sensors,"
Proc. SPIE, vol. 10646 Apr. 2018, Art. no. 1064605.

[4] D. Belfadel, Y. Bar-Shalom, and P. Willett
"Simultaneous target state and passive sensors bias estimation,"
in *Proc. 19th Int. Conf. FUSION*, 2016, pp. 1223–1227.

[5] D. Belfadel, R. W. Osborne, and Y. Bar-Shalom
"Bias estimation and observability for optical sensor measurements with targets of opportunity,"
J. Adv. Inf. Fusion, vol. 9, no. 2, pp. 59–74, Dec. 2014.

[6] D. Belfadel, R. W. Osborne, and Y. Bar-Shalom
"Bias estimation for moving optical sensor measurements with targets of opportunity,"
J. Adv. Inf. Fusion, vol. 10, no. 2, pp. 101–112, Dec. 2015.

[7] T. M. Clemons and K.-C. Chang
"Effect of sensor bias on space-based bearings-only tracker,"
Proc. SPIE, vol. 6968, Aug. 2008, Art. no. 696809.

[8] T. M. Clemons and K.-C. Chang
"Sensor calibration using in-situ celestial observations to estimate bias in space-based missile tracking,"
IEEE Trans. Aerosp. Electron. Syst., vol. 48, no. 2, pp. 1403–1427, Apr. 2012.

[9] B. D. Kragel, S. Danford, S. M. Herman, and A. B. Poore
"Bias estimation using targets of opportunity,"
Proc. SPIE, vol. 6699, Aug. 2007, Art. no. 66991F.

[10] S. D. Ma
"A self-calibration technique for active vision systems,"
IEEE Trans. Robot. Automat., vol. 12, no. 11, pp. 114–120, Feb. 1996.

[11] R. W. Osborne, III and Y. Bar-Shalom
"Statistical efficiency of composite position measurements from passive sensors,"
in *Proc. SPIE Conf. Signal and Data Processing of Small Targets Recognition XX*, #805008, Orlando, FL, May 2011. https://doi.org/10.1117/12.883045

[12] R. W. Osborne, III and Y. Bar-Shalom
"Statistical efficiency of composite position measurements from passive sensors,"
IEEE Tans. Aerosp. Electron. Syst., vol. 49, no. 4, pp. 2799–2806, Oct. 2013.

[13] Z. Zhang
"A flexible new technique for camera calibration,"
IEEE Trans. Pattern Anal. Mach. Intell., vol. 22, no. 11, pp. 1330–1334, Nov. 2000.

[14] Z. Zhang
"Camera calibration with one-dimensional objects,"
in *Proc. Eur. Conf. Comput. Vision*, 2002, pp. 161–174.

Djedjiga Belfadel received the Ph.D. degree in electrical and computer engineering from the University of Connecticut, Storrs, CT, USA. in 2015. She is currently an Associate Professor in the Electrical and Biomedical Engineering Department, Fairfield University, Fairfield, CT, USA. Her research traverses a wide breadth of estimation theory, with a specific emphasis on practical applications such as drone navigation and target tracking. Her scholarly contributions extend to space-based infrared (IR) and electro-optical (EO) sensors, signal and image processing, machine learning, and big data. Alongside her research, she is committed to enhancing engineering education and boosting the representation of women and underrepresented groups within the engineering sector.